Letters

Spread-Spectrum Technique Employing Phase-Shift Modulation to Reduce EM Noise for Parallel–Series LLC Resonant Converter

Hwa-Pyeong Park, *Student Member, IEEE*, Mina Kim, *Student Member, IEEE*, and Jee-Hoon Jung, *Senior Member, IEEE*

***Abstract*—A spread-spectrum technique (SST) has been developed to mitigate an electromagnetic interference in power converters. However, for resonant converters using a pulse-frequency modulation, it is difficult to regulate its output voltage with the SST, because the switching-frequency variation according to the spread spectrum induces large output-voltage fluctuation. In this letter, an enhanced phase-shift algorithm of the frequency modulation of the SST and a parallel–series structure for an LLC resonant converter are proposed to obtain a tight output-voltage regulation under the spread-spectrum operation. The performance of the proposed methods is experimentally verified using a 600-W prototype parallel–series LLC resonant converter.**

***Index Terms*—Electromagnetic interference (EMI), LLC resonant converter, output-voltage regulation, spread spectrum.**

I. Introduction

ALL the electric products should satisfy electromagnetic interference (EMI) standards to be released to market [1]. Therefore, EMI reduction has been a significant issue for designing and implementing switch-mode power supplies (SMPS). Passive and active EMI filters, printed circuit board (PCB), design, soft-switching techniques, and spread-spectrum techniques (SST) have been developed to suppress the electromagnetic (EM) noise [2]–[7]. Large EMI filters can satisfy the EMI standards; however, they show poor cost effectiveness and size increment of the SMPS. In addition, the soft-switching techniques depend on converter topologies. The SST has been introduced to suppress the EM noise with preshaped switching patterns, which have several technical branches, such as sinusoidal, triangular, Hershey-kiss, and random modulations [8]. The frequency modulation of the SST can be expressed as follows [9]:

$$s(t) = A_o \cos\left[2\pi f_c t + 2\pi \Delta f \int_{-\infty}^{t} \xi(\tau)\, d\tau\right] \quad (1)$$

where A_o is the signal amplitude, $\xi(\tau)$ $(-1 \leq \xi \leq 1)$ is the preshaped switching pattern, and Δf is the frequency deviation of the SST. The SST distributes the switching frequency with the preshaped pattern

Manuscript received April 11, 2018; revised May 11, 2018 and June 5, 2018; accepted June 24, 2018. Date of publication June 26, 2018; date of current version December 7, 2018. This work was supported in part by the "Development of pilot-level facility and testing board for Seawater Battery" Research Fund of EWP (Korea East-West Power Co., Ltd.) and in part by the National Research Foundation of Korea under Grant NRF-2016R1A2B4011934. *(Corresponding author: Jee-Hoon Jung.)*

The authors are with the School of Electrical and Computer Engineering, Ulsan National Institute of Science and Technology, Ulsan 44919, South Korea (e-mail:

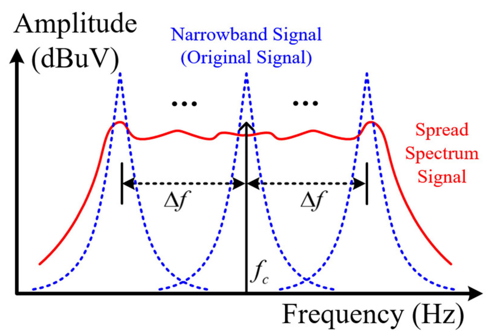

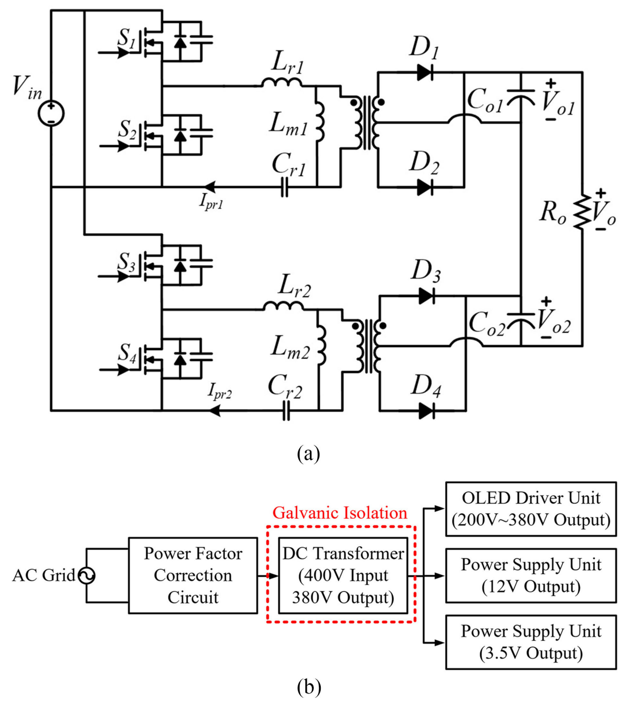

Fig. 2. Schematic of the proposed converter and system. (a) Parallel–series LLC resonant converter. (b) Entire input-power structure of OLED TV.

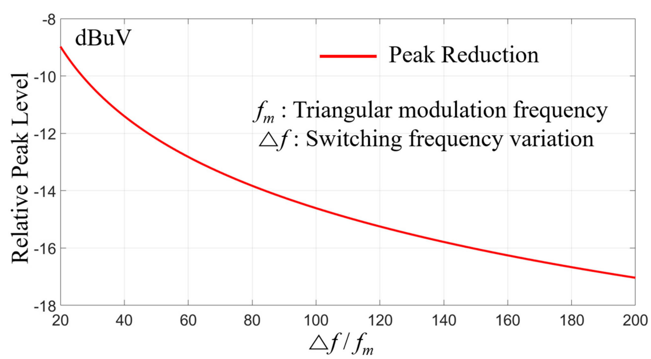

Fig. 3. Relative peak level of conducted emission EMI according to $\Delta f/f_{\mathrm{m}}$.

modulation case. The operational principles of the proposed parallel–series LLC resonant converter employing the phase-shift algorithm will be analyzed to obtain design considerations and to estimate performance improvement. The output-voltage regulation and the EMI-reduction performances using the SST will be experimentally verified with a 600-W prototype parallel–series LLC resonant converter.

II. Proposed SST and Converter Structure

Fig. 2(a) shows the schematic of the parallel–series LLC resonant converter, which has a parallel connection on the primary side and a series connection on the secondary side. The target application of the converter is a dc transformer for flat-panel display applications, especially an organic LED (OLED) television (TV), which has the specification of 400 V input voltage and 380 V output voltage [18]. Fig. 2(b) shows the entire input-power structure of the OLED TV, which requires the dc transformer to achieve a galvanic isolation between the

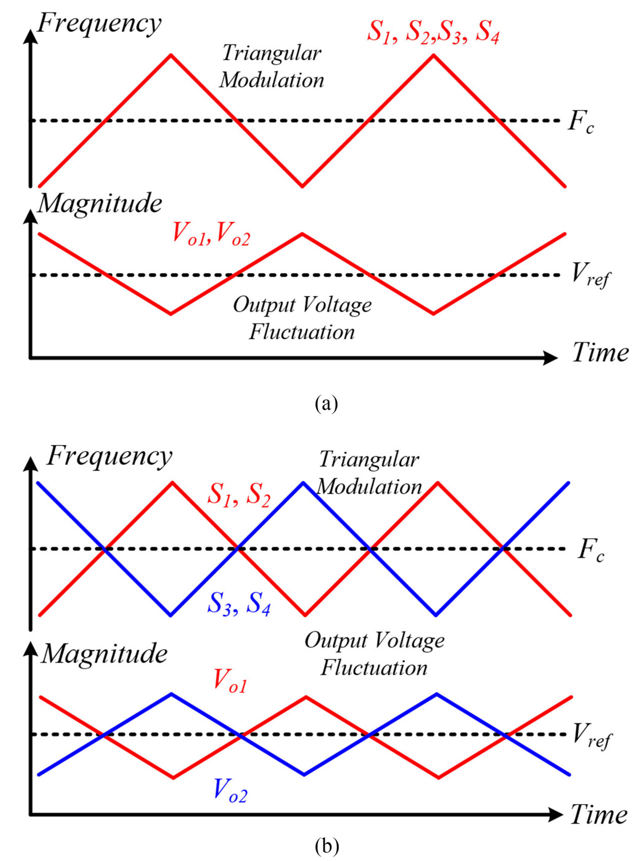

Fig. 4. Theoretical operating waveforms of the parallel–series LLC resonant converter employing the SST. (a) With the conventional inphase modulation. (b) With the proposed phase-shift algorithm.

ac grid to the TV side. In addition, the OLED driver requires high input voltage (380 V) and low input current (1.2 A).

A. Compensation Algorithm for Output-Voltage Regulation Under SST

The SST can reduce the peak values of the EM noise, which is well introduced in [8] and [9]. Fig. 3 shows the reduction of relative peak levels of conducted emission EMI according to $\Delta f/f_{\mathrm{m}}$ ratio. Using the wider switching-frequency variation (Δf) and the lower triangular modulation frequency (f_{m}), the converter employing the SST can obtain the higher EMI-reduction performance. In addition, the designed f_{m} should be higher than the resolution bandwidth of the spectrum analyzer to obtain the EM-noise reduction theoretically [19]. In this letter, the desired reduction level of the EMI peak is 10 dBμV comparing with the case without the SST.

The SST requires a wide switching-frequency variation to reduce the EM noise. The LLC resonant converter has serious output-voltage fluctuation caused by the SST, since the voltage gain of the converter is determined by the switching frequency. The voltage gain of the LLC resonant converter can be derived as follows [20]:

$$G(f_{\mathrm{n}}) = \left| \frac{\lambda^{-1} f_{\mathrm{n}}^{\,2}}{(\lambda^{-1}+1)\, f_{\mathrm{n}}^{\,2} - 1 + j\left(f_{\mathrm{n}}^{\,2} - 1\right) f_{\mathrm{n}}^{\,-1}} \right| \tag{2}$$

where λ is the resonant inductance and magnetizing inductance ratio and f_{n} is the normalized frequency. The output-voltage variation

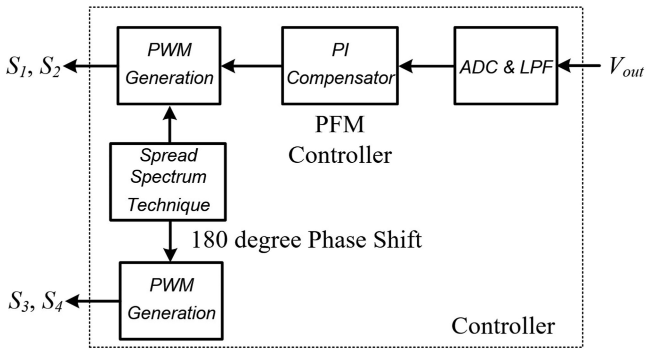

Fig. 5. Control block diagram of the proposed phase-shift algorithm and SST.

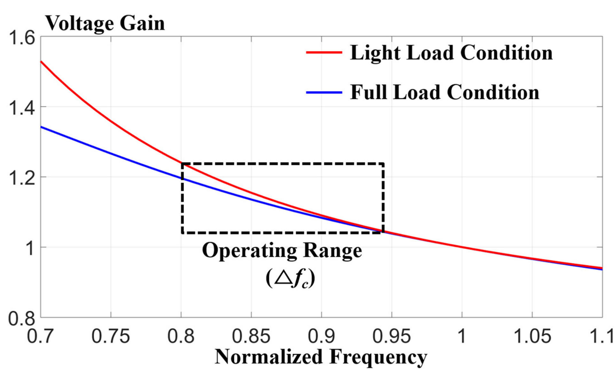

(a)

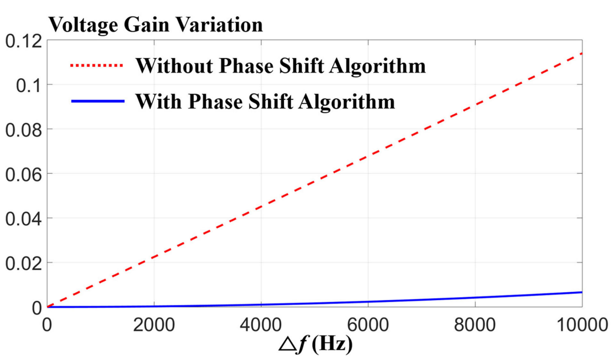

(b)

Fig. 6. Voltage-gain variation according to compensation by phase-shift algorithm.

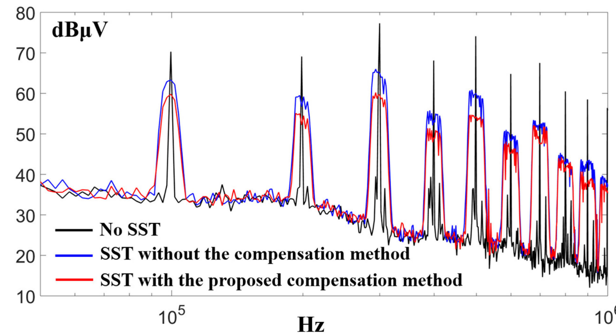

(a)

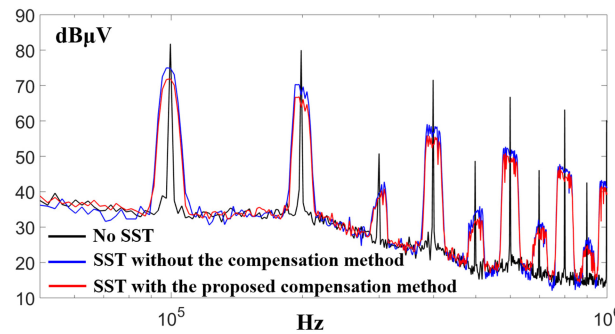

(b)

Fig. 7. Experimental measurements of conducted emission EMI reduction performance. (a) Common-mode noise. (b) Differential-mode noise.

TABLE I
DESIGN SPECIFICATIONS

Parameter	Experimental Value
V_{in}	400 V
Rate Load Condition	380 V, 1.58 A
Resonant Capacitance	36 nF
Resonant Inductance	83 μH
Magnetizing Inductance	290 μH
f_s	89 kHz
Δf	13.5 kHz
f_m	450 Hz

according to the SST can be derived as follows:

$$\Delta V_{\mathrm{o,max}} = \frac{[G(f_{\mathrm{c}} + \Delta f_{\mathrm{max}}) - G(f_{\mathrm{c}} - \Delta f_{\mathrm{max}})] \cdot V_{\mathrm{in}}}{n} \quad (3)$$

where $G(f)$ is the input-to-output voltage gain of the LLC resonant converter, V_{in} is the input voltage, Δf_{max} is the maximum switching-frequency variation, and n is the transformer's turn ratio. It shows that the wider switching-frequency variation induces larger output-voltage fluctuation.

Fig. 4(a) shows the theoretical operating waveforms of the switching-frequency variation and the output-voltage fluctuation of the converter according to the SST. In this case, the power converter uses a conventional inphase modulation for the SST. All the switching legs have the same pattern according to the switching-frequency variation, which induces the same fluctuation shape of the output voltages (V_{o1} and V_{o2}). It becomes the sum of V_{o1} and V_{o2} because of the series connection in the secondary output. The output-voltage fluctuation of the parallel–series LLC resonant converter employing the SST can be derived as follows:

$$\Delta V_{\mathrm{o,c}} = [G(f_{\mathrm{c}} - \Delta f) - G(f_{\mathrm{c}} + \Delta f)] \cdot \left(\frac{V_{\mathrm{in}}}{n_1} + \frac{V_{\mathrm{in}}}{n_2}\right) \quad (4)$$

where $\Delta V_{\mathrm{o,c}}$ is the output voltage fluctuation under the conventional in-phase modulation, and n_1 and n_2 are the transformer turn ratios. Therefore, the same variation of V_{o1} and V_{o2} induces serious output-voltage fluctuation without any compensation method.

The parallel–series structure of the converter and the phase-shift algorithm of the SST can solve this output-voltage-fluctuation problem under the spread-spectrum operation. The parallel–series structure can independently control each output voltage of V_{o1} and V_{o2}. In addition, the performance of the output-voltage regulation is determined by out-of-phase between V_{o1} and V_{o2}. Fig. 4(b) shows the theoretical operating waveforms of the proposed phase-shift algorithm and the output-voltage fluctuation. The first converter shows inphase switching pattern

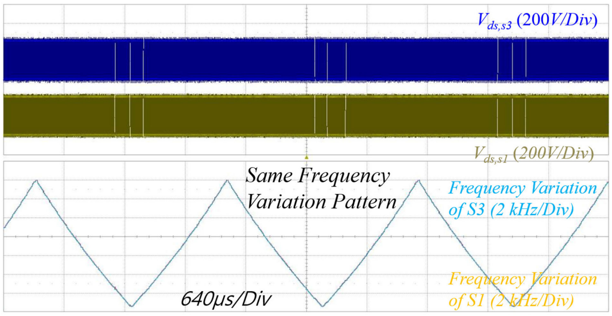

(a)

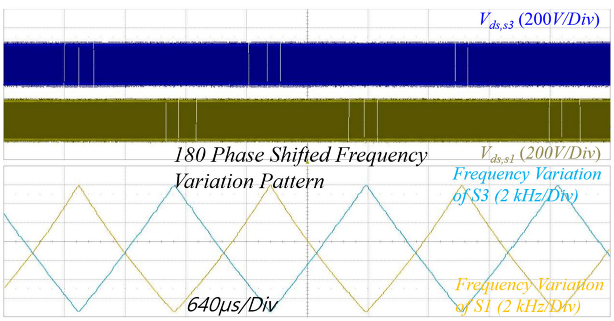

(b)

Fig. 8. Experimental operating waveforms using the proposed phase-shift algorithm of the SST.

of the SST. The second converter shows 180°-phase-shifted switching pattern of the SST. The phase-shifted switching pattern generates 180°-phase-shifted voltage variation according to the first converter. When n_1 and n_2 are the same turn ratio, the output-voltage fluctuation using the proposed algorithm and structure can be expressed as follows:

$$\Delta V_{\mathrm{o,p}} = \left[\frac{G\left(f_{\mathrm{c}} + \Delta f\right) + G\left(f_{\mathrm{c}} - \Delta f\right)}{2} - G\left(f_{\mathrm{c}}\right)\right] \frac{V_{\mathrm{in}}}{n} \tag{5}$$

where $\Delta V_{\mathrm{o,p}}$ shows the amount of the voltage variation using the proposed algorithm and structure, which is ideally compensated to zero. Fig. 5 shows the control block diagram of the proposed phase-shift algorithm of the SST to mitigate the EM noise and to improve the output-voltage regulation. The digital controller (TI TMS320F28335) is used to implement the proposed phase-shift algorithm and the SST.

B. Design Considerations of Voltage Gain

The voltage gain of the LLC resonant converter is nonlinear. The proposed phase-shift algorithm for the SST cannot make the output-voltage ripple zero. The analysis of the output-voltage variation according to the SST is significant to design the resonant network of the converter. The LLC resonant converter has nonlinear voltage-gain curve. Using (4) and (5), Fig. 6(a) and (b) show the voltage-gain variation using the proposed phase-shift algorithm comparing with the conventional inphase modulation case. The voltage-gain variation with the conventional inphase modulation is ten times larger than that with the proposed phase-shift algorithm. In addition, they show a larger output-voltage fluctuation under the wider frequency variation caused by the nonlinear characteristic of the voltage gain.

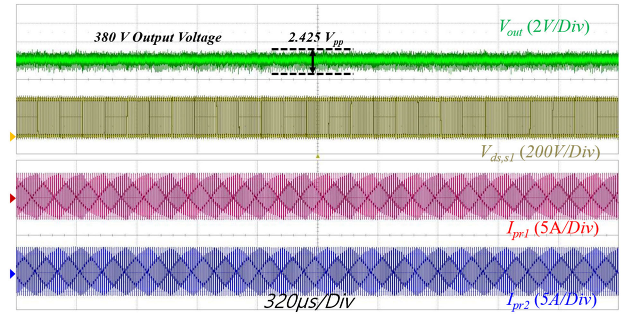

(a)

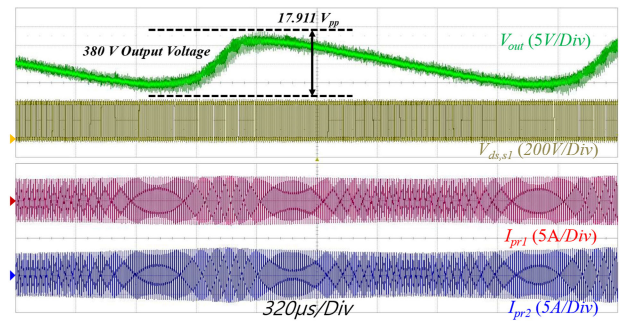

(b)

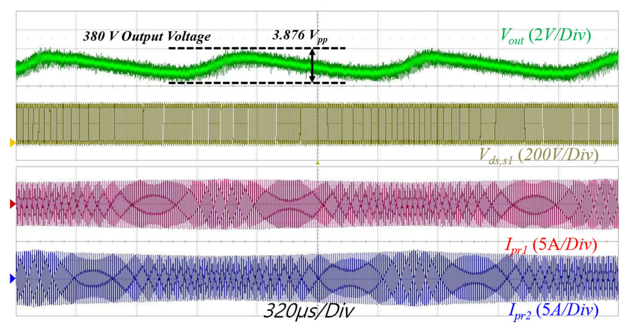

(c)

Fig. 9. Experimental waveforms of output voltage, switch voltage, and primary and secondary currents. (a) No SST. (b) Using SST with inphase modulation. (c) Using SST with the proposed phase-shift algorithm.

III. Experimental Results

Fig. 7(a) and (b) show the quasi-peak values of common-mode-(CM) and differential-mode-(DM) conducted emission EM noises, respectively. From Fig. 7, using the SST, all the EM noise can effectively be reduced. The proposed phase-shift algorithm has a better EM-noise reduction performance than that of the inphase modulation, since the smaller output-voltage fluctuation induces the smaller dv/dt and di/dt in the output capacitor and the resonant tank [21]. Table I provides detail specifications of the 600-W prototype parallel–series LLC resonant converter and the employed SST used in the experiments. Fig. 8(a) shows the in-phase modulation waveform. Fig. 8(b) shows the proposed phase-shift algorithm of the SST, which has a 180° phase shift of the switching-frequency variation of the SST between two converters. Fig. 9 shows the output-voltage regulation performance according to the operating cases. Fig. 9(a)–(c) show the steady-state operating waveforms of no SST, using the SST with the conventional inphase modulation, and using the SST with the proposed phase-shift algorithm, respectively. Without the SST, the output-voltage ripple is 2.425 V_{pp}. Using the SST and the inphase modulation, the voltage ripple is 17.911 V_{pp} which is 7.4 times higher than that of the no-SST case. Us-

TABLE II
PERFORMANCE COMPARISON

Measured Results	No SST	SST with in-phase modulation
Peak CM noise	67.2 dBμV	54.9 dBμV
Peak DM noise	71.7 dBμV	64.9 dBμV
Output Voltage Ripple	2.425 V_{pp}	17.911 V_{pp}
Measured Results		SST with phase-shift algorithm
Peak CM noise		50.1 dBμV
Peak DM noise		61.9 dBμV
Output Voltage Ripple		3.876 V_{pp}

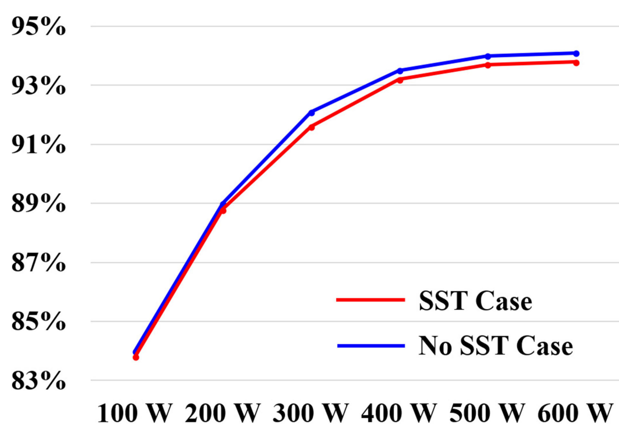

Fig. 10. Power conversion efficiency.

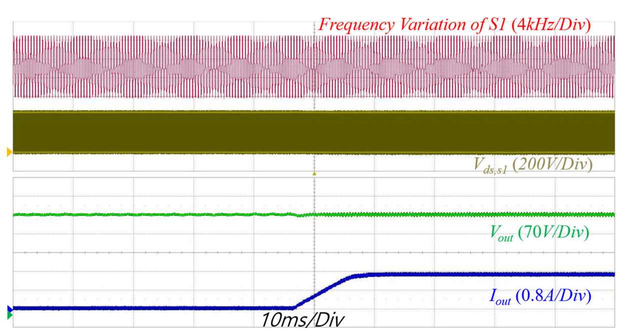

Fig. 11. Step-load response under operating the proposed phase-shift algorithm.

ing the SST with the proposed algorithm, the voltage ripple is 3.876 V_{pp} which is 4.6 times smaller than that of the inphase modulation case. Table II provides the performance comparison of the EMI reduction and the output-voltage regulation using the SST with the proposed algorithm. The proposed algorithm can achieve a tight output-voltage regulation than that of inphase modulation. In addition, it has low EM noise than that of the no-SST case.

The LLC resonant converter designed using the specifications of Table I has zero voltage switching and zero current switching capabilities for all the operating range. The SST has higher conduction loss than that of the no-SST case. The conduction loss of the SST case can be expressed as follows:

$$P_{\mathrm{c,sst}} = \frac{R_{\mathrm{p}}}{2}\left\{\left[\frac{G\left(f_c-\Delta f\right)V_{\mathrm{in}}}{R_{\mathrm{out}}}\right]^2+\left[\frac{G\left(f_c+\Delta f\right)V_{\mathrm{in}}}{R_{\mathrm{out}}}\right]^2\right\} \quad (6)$$

where R_{out} is the load resistance, and R_{p} is the parasitic resistance of the power stage. Fig. 10 shows the measured curve of power-conversion efficiency. It verifies that the SST induces higher power loss than that of the no-SST case. Fig. 11 shows the operational waveform during step-load change. The proposed phase-shift algorithm can continuously operate the SST during the load variation.

IV. CONCLUSION

In this letter, the phase-shift algorithm of the SST and the parallel–series structure of the LLC resonant converters are proposed to obtain the EMI reduction and a tight output-voltage regulation simultaneously. This shows four major contributions as follows:

First, the proposed phase-shift algorithm of the switching-frequency modulation in the SST is shown to effectively improve the output-voltage-regulation performance compared with that of the conventional inphase modulation. Second, the parallel–series structure of the LLC resonant converters is a significant contribution of this letter to reduce the output-voltage fluctuation according to the SST. Third, the proposed phase-shift algorithm applied to the SST can improve the EMI-reduction performance as well as the output-voltage regulation. Finally, the combination of proposed interleaving method and SST for the LLC resonant converter is the first trial to reduce the EM noise and the output-voltage fluctuation.

The operational principles of the proposed algorithm and structure are analyzed to obtain the design methodology and estimate their performance improvements. The experimental results show the reduction of the conducted emission EM noises (-9.8 dBμV on DM and -17.1 dBμV on CM). In addition, the proposed phase-shift algorithm shows 4.6 times smaller output-voltage fluctuation than the case of using the SST with the conventional inphase modulation.

REFERENCES

[1] FCC, "Code of federal regulations 47 (47CFR), part 15, subpart b: Unintentional radiators," 2017. [Online]. Available: http://www.ecfr.gov/. Accessed on: Jun. 27, 2017.
[2] K. Raggl, T. Nussbaumer, and J. W. Kolar, "Guideline for a simplified differential-mode EMI filter design," *IEEE Trans. Ind. Electron.*, vol. 57, no. 3, pp. 1031–1040, Mar. 2010.
[3] M. C. D. Piazza, A. Ragusa, and G. Vitale, "Power-loss evaluation in CM active EMI filters for bearing current suppression," *IEEE Trans. Ind. Electron.*, vol. 58, no. 11, pp. 5142–5153, Nov. 2011.
[4] H. Chung, S. Y. R. Hui, and K. K. Tse, "Reduction of power converter EMI emission using soft-switching technique," *IEEE Trans. Electromagn. Compat.*, vol. 40, no. 3, pp. 282–287, Aug. 1998.
[5] D. G. *et al.*, "Conducted EMI reduction in power converters by means of periodic switching frequency modulation," *IEEE Trans. Power Electron.*, vol. 22, no. 6, pp. 2271–2281, Nov. 2007.
[6] K. K. Tse, H. S. H. Chung, S. Y. Huo, and H. C. So, "Analysis and spectral characteristics of a spread-spectrum technique for conducted EMI suppression," *IEEE Trans. Power Electron.*, vol. 15, no. 2, pp. 399–410, Mar. 2000.
[7] O. Trescases, G. Wei, A. Prodic, and W. T. Ng, "An EMI reduction technique for digitally controlled SMPS," *IEEE Trans. Power Electron.*, vol. 22, no. 4, pp. 1560–1565, Jul. 2007.
[8] F. Pareschi, R. Rovatti, and G. Setti, "EMI reduction via spread spectrum in DC/DC converters: State of the art, optimization, and tradeoffs," *IEEE Acess.*, vol. 3, pp. 2857–2874, 2015.
[9] F. Pareschi, G. Setti, R. Rovatti, and G. Frattini, "Practical optimization of EMI reduction in spread spectrum clock generators with application to switching DC/DC converters," *IEEE Trans. Power Electron.*, vol. 29, no. 9, pp. 4646–4657, Sep. 2014.
[10] L. A. Barragan, D. Navarro, J. Acero, I. Urriza, and J. M. Burdio, "FPGA implementation of a switching frequency modulation circuit for EMI reduction in resonant inverters for induction heating appliances," *IEEE Trans. Ind. Electron.*, vol. 55, no. 1, pp. 11–20, Jan. 2008.
[11] H. P. Park, M. Kim, and J. H. Jung, "Spread spectrum technique to reduce emi emission for an LLC resonant converter using a hybrid modulation method," *IEEE Trans. Power Electron.*, vol. 33, no. 5, pp. 3717–3721, May 2018.

[12] M. I. Shahzad, S. Iqbal, and S. Taib, “Interleaved LLC converter with cascaded voltage-doubler rectifiers for deeply depleted PEV battery charging,” in *Proc. IEEE Trans. Transp. Electrific.*, vol. 4, no. 1, pp. 89–98, Mar. 2018.

[13] H. Wu, X. Zhan, and Y. Xing, “Interleaved LLC resonant converter with hybrid rectifier and variable-frequency plus phase-shift control for wide output voltage range applications,” *IEEE Trans. Power Electron.*, vol. 32, no. 6, pp. 4246–4257, Jun. 2017.

[14] K. Murata and F. Kurokawa, “An interleaved PFM LLC resonant converter with phase-shift compensation,” *IEEE Trans. Power Electron.*, vol. 31, no. 3, pp. 2264–2272, Mar. 2016.

[15] X. Sun, Y. Shen, Y. Zhu, and X. Guo, “Interleaved boost-integrated LLC resonant converter with fixed-frequency PWM control for renewable energy generation applications,” *IEEE Trans. Power Electron.*, vol. 30, no. 8, pp. 4312–4326, Aug. 2015.

[16] Z. Hu, Y. Qiu, Y. F. Liu, and P. C. Sen, “A control strategy and design method for interleaved LLC converters operating at variable switching frequency,” *IEEE Trans. Power Electron.*, vol. 29, no. 8, pp. 4426–4437, Aug. 2014.

[17] K. H. Yi and G. W. Moon, “Novel two-phase interleaved LLC series-resonant converter using a phase of the resonant capacitor,” *IEEE Trans. Ind. Electron.*, vol. 56, no. 5, pp. 1815–1819, May 2009.

[18] P. Y. Huang, C. S. Leu, W. C. Lin, and K. H. Liao, “LLC converter with Taiwan Tech voltage doubler rectifier (LLC-TVD) for large-size LED-backlit LCD display applications,” in *Proc. Int. Future Energy Electron. Conf.*, vol. 1, 2013, pp. 618–622.

[19] Y. Matsumoto, S. Ishigami, and K. Gotoh, “4-3 effects of spread spectrum clocking on measured noise spectra,” *J. Nat. Inst. Inf. Commun. Technol.*, vol. 53, no. 1, pp. 101–115, Oct. 2006.

[20] H. P. Park and J. H. Jung, “Power stage and feedback loop design for LLC resonant converter in high-switching-frequency operation,” *IEEE Trans. Power Electron.*, vol. 32, no. 10, pp. 7770–7782, Oct. 2017.

[21] B. Mammano and B. Carsten, “Understanding and optimizing electromagnetic compatibility in switch-mode power supplies,” in *Proc. Unitrode Power Supply Des. Semin. Topics*, vol. 1, 2002, pp. 1–17.